Audio Engineering Society

Convention Paper

Presented at the 126th Convention
2009 May 7–10   Munich, Germany

Spatial Sampling Artifacts of Wave Field Synthesis for the Reproduction of Virtual Point Sources

Sascha Spors and Jens Ahrens

Deutsche Telekom Laboratories, Technische Universität Berlin, Ernst-Reuter-Platz 7, 10587 Berlin, Germany

Correspondence should be addressed to Sascha Spors (`Sascha.Spors@telekom.de`)

ABSTRACT

Spatial sound reproduction systems with a large number of loudspeakers are increasingly being used. Wave field synthesis is a reproduction technique using a large number of densely placed loudspeakers (loudspeaker array). The underlying theory, however, assumes a continuous distribution of loudspeakers. Individual loudspeakers placed at discrete positions constitute a spatial sampling process that may lead to sampling artifacts. These may degrade the perceived reproduction quality and will limit the application of active control techniques like active room compensation. The sampling artifacts for the reproduction of plane waves have already been discussed in previous papers. This paper derives the spatial sampling artifacts and anti-aliasing conditions for the reproduction of virtual point sources on linear loudspeaker arrays using wave field synthesis techniques.
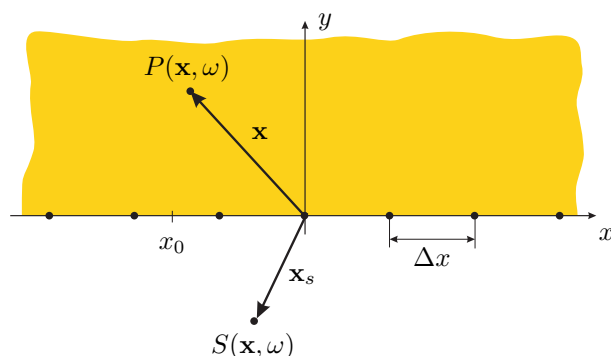
1. INTRODUCTION

High-resolution sound reproduction aims at creating the perfect acoustic illusion of an existing or virtual acoustic space. Various reproduction systems with a varying number of loudspeaker channels emerged over the past decades in order to achieve this goal. An interesting class, within these approaches, are those systems who are based on the concept of physically reproducing the sound of complex acoustic scenes as natural as possible. One of the proposed methods is wave field synthesis (WFS). In theory, WFS creates an almost physically correct reproduction of almost any virtual wave field by a continuous distribution of acoustic sources (secondary sources) placed around the listening area. In practical implementations this distribution will be realized by a limited number of loudspeakers placed at discrete positions. This spatial sampling of the continuous

secondary source distribution may lead to spatial sampling artifacts that corrupt the physical correct reproduction of the desired virtual source.

Typical implementations of WFS systems are based on (piecewise) linear loudspeaker arrays. A detailed analysis of spatial aliasing artifacts for the reproduction of plane waves has already been published [1, 2, 3]. The frequency domain description of time domain sampled signals, by way of their Fourier transformation, has proven to be a powerful tool for the description of time-domain aliasing artifacts. A similar route has been chosen to analyze the effects of spatial sampling in sound reproduction. By interpreting acoustic wave fields as multidimensional signals and modeling the spatial sampling similar to time-domain sampling a rigid formulation of the spatial sampling effects has been derived. Such a rigorous analysis for the reproduction of virtual point sources is currently missing to the knowledge of the authors.

This paper analyzes the spatial sampling artifacts for the reproduction of virtual point sources using linear loudspeaker arrays. The underlying frequency domain description allows to conveniently identify the aliasing contributions in the reproduced wave field. It is further shown, that the truncation of the secondary source distribution as occurring in practical implementations plays an important role in the analysis of spatial sampling artifacts. The appearance of spatial aliasing depends on the position of the virtual source and the listener with respect to the truncated loudspeaker array. Based on the derived results anti-aliasing conditions are formulated. The spatial sampling artifacts have implications on (1) the objective and subjective reproduction quality, and (2) the application of active control techniques. Recent results from subjective experiments carried out with typical WFS systems revealed that spatial aliasing artifacts can be perceived as coloration of the virtual source [4]. However, the underlying psychoacoustic mechanisms are not clear at the current stage. A detailed analysis of spatial aliasing artifacts may help to design appropriate subjective experiments and to understand the psychoacoustic mechanisms. The performance of active control applications like active listening room compensation (ARC), active noise control (ANC) and acoustic echo cancelation (AEC) will be limited by spatial aliasing. A detailed analysis of spatial aliasing artifacts

Fig. 1: Geometry used to derive the sampling artifacts for linear loudspeaker arrays. The ● denote the sampling positions of the driving function $D_S(x, \omega)$ and the colored plane the reproduction area $(y > 0)$.

helps to predict the performance of such techniques.

2. WAVE FIELD SYNTHESIS

The theory of WFS has been initially developed at the Technical University of Delft [5]. A vivid research community and a number of practical implementations has evolved since then. The authors have recently published an overview of the theory [6] that serves as basis for the theoretical background of WFS as presented here.

2.1. Basic Theory

Its mathematical foundation for three-dimensional arbitrary shaped volumes is given by the Kirchhoff-Helmholtz integral [7, 5]. Typical implementations of WFS systems are restricted to the reproduction in a plane only using (piecewise) linear loudspeaker arrays. The theoretical basis for this situation is given by the two-dimensional Rayleigh I integral [7, 5]. The Rayleigh I integral states that a linear distribution of monopole line sources (secondary sources) is capable of reproducing a desired wave field (virtual source) in one of the half planes defined by the linear distribution. The wave field in the other half plane is a mirrored version of the desired wave field. Without loss of generality the geometry depicted in Fig. 1 is assumed: A linear secondary source distribution which is located on the x-axis $(y = 0)$ of a Cartesian coordinate system. The reproduced wave field is given by specializing the two-dimensional

Rayleigh I integral [8]

$$P(\mathbf{x}, \omega) = - \int_{-\infty}^{\infty} D(\mathbf{x}_0, \omega) G(\mathbf{x} - \mathbf{x}_0, \omega) dx_0 \ , \quad (1)$$

where $\mathbf{x} = [x \, y]^T$ with $y > 0$ and $\mathbf{x}_0 = [x_0 \, 0]^T$. The functions $D(\mathbf{x}_0, \omega)$ and $G(\mathbf{x} - \mathbf{x}_0, \omega)$ denote the (secondary source) driving function and the wave field of the secondary sources, respectively. For two-dimensional reproduction the wave field of the secondary sources is given by the two-dimensional free-field Green's function

$$G(\mathbf{x} - \mathbf{x}_0, \omega) = \frac{j}{4} H_0^{(2)}(\frac{\omega}{c} |\mathbf{x} - \mathbf{x}_0|) \ , \qquad (2)$$

where $H_0^{(2)}(\cdot)$ denotes the Hankel function of second kind and zeroth-order [9]. Equation (2) can be interpreted as the field of a line source intersecting the listening area at the position $\mathbf{x}_0$.

The secondary source driving function is given as

$$D(\mathbf{x}_0, \omega) = 2 \frac{\partial}{\partial \mathbf{n}} S(\mathbf{x}, \omega) \Big|_{\mathbf{x} = \mathbf{x}_0} \ , \qquad (3)$$

where $\frac{\partial}{\partial \mathbf{n}}$ denotes the directional gradient with $\mathbf{n} = [0 \, 1]^T$. We aim at investigating the spatial sampling artifacts for virtual point sources in this paper. The analogon to monopole point sources in three-dimensional wave propagation are in two dimensions monopole line sources. Hence, the wave field of the virtual source is given by the wave field of a line source

$$S(\mathbf{x}, \omega) = \frac{j}{4} H_0^{(2)}(\frac{\omega}{c} |\mathbf{x} - \mathbf{x}_s|) \ , \qquad (4)$$

where $\mathbf{x}_s = [x_s \, y_s]^T$ denotes the position of the line source with $y_s < 0$.

We will rely on the theory of two-dimensional WFS, as introduced above, for the derivation of the sampling artifacts . We will assume that the secondary sources have the characteristics of line sources. Practical implementations of WFS systems use closed loudspeakers as secondary sources. These approximately have the characteristics of acoustic point sources. This mismatch in source types may produce various artifacts in the reproduced wave field that can only be corrected to some extend [7, 10]. This technique is known as 2.5D WFS.

Within this paper, the effects of sampling are derived for two-dimensional WFS with line sources as

secondary sources. It was shown in [2, 11] that the anti-aliasing conditions derived for plane waves and two-dimensional WFS hold also for 2.5D reproduction.

2.2. Spatio-temporal Frequency Domain Representation

The reproduced wave field is given, according to Eq. (1) and (2), as a convolution along the x-axis. The driving function $D(\mathbf{x}, \omega)$ is convolved with the secondary source wave field $G(\mathbf{x} - \mathbf{x}_0, \omega)$. Applying a spatial Fourier transformation to Eq. (1) with respect to the x-coordinate results in

$$\tilde{P}(k_x, y, \omega) = -\tilde{D}(k_x, \omega) \tilde{G}(k_x, y, \omega) \ , \qquad (5)$$

where k_x denotes the spatial frequency (wave number), spatial frequency domain quantities are denoted by a tilde over the respective variable. The spatial Fourier transformation of $P(\mathbf{x}, \omega)$ is defined as

$$\tilde{P}(k_x, y, \omega) = \int_{-\infty}^{\infty} P(\mathbf{x}, \omega) \, e^{j k_x x} dx \ . \qquad (6)$$

The Fourier transformation of $D(\mathbf{x}, \omega)$ is defined accordingly, the Fourier transformation $\tilde{G}(k_x, y, \omega)$ is given by transforming $G(\mathbf{x} - \mathbf{x}_0, \omega)$ for $\mathbf{x}_0 = \mathbf{0}$.

Equation (5) reveals that the spatial convolution is represented by a scalar multiplication in the spatial frequency domain. This representation has been proven to be very efficient in the calculation of the reproduced wave field and the description of secondary source sampling [2, 3, 1, 12, 7]. However, the spatial Fourier transform of the driving function and the secondary source are required for specific results. These will be derived in the following.

Both, the description of the secondary sources given by (2) and the desired virtual line source (4) contain the Hankel function $H_0^{(2)}(\cdot)$. The spatial Fourier transform, with respect to the x-coordinate, of the Hankel function $H_0^{(2)}(\frac{\omega}{c} |\mathbf{x} - \mathbf{x}_0|)$ can be computed by exploiting the symmetry of the involved functions, applying suitable substitutions and using the integrals [13, 6.677-3/4]. It is given as

$$\mathcal{F}_x \{ H_0^{(2)}(\frac{\omega}{c} |\mathbf{x} - \mathbf{x}_0|) \} = e^{j k_x x_0} \times$$

$$\times \begin{cases} \frac{2}{\sqrt{(\frac{\omega}{c})^2 - k_x^2}} \, e^{-j \sqrt{(\frac{\omega}{c})^2 - k_x^2} \, (y - y_0)} & \text{for } |k_x| < \left| \frac{\omega}{c} \right| \ , \\ \frac{2j}{\sqrt{k_x^2 - (\frac{\omega}{c})^2}} \, e^{-\sqrt{k_x^2 - (\frac{\omega}{c})^2} \, (y - y_0)} & \text{for } \left| \frac{\omega}{c} \right| < |k_x| \ , \end{cases}$$

$$(7)$$

which is valid for $y > y_0$.

The spatial Fourier transformation of the secondary sources $\tilde{G}(k_x, y, \omega)$ is given by multiplying Eq. (7) with $j/4$ and introducing $\mathbf{x}_0 = \mathbf{0}$

$$\tilde{G}(k_x, y, \omega) = \begin{cases} \frac{j}{2} \frac{e^{-j\sqrt{(\frac{\omega}{c})^2 - k_x^2}\, y}}{\sqrt{(\frac{\omega}{c})^2 - k_x^2}} & \text{for } |k_x| < \left|\frac{\omega}{c}\right| , \\ -\frac{1}{2} \frac{e^{-\sqrt{k_x^2 - (\frac{\omega}{c})^2}\, y}}{\sqrt{k_x^2 - (\frac{\omega}{c})^2}} & \text{for } \left|\frac{\omega}{c}\right| < |k_x| , \end{cases} \tag{8}$$

which is valid for $y > 0$. The spectrum $\tilde{G}(k_x, y, \omega)$ consists of two contributions: a traveling wave contribution for $|k_x| < \left|\frac{\omega}{c}\right|$ and an evanescent contribution for $\left|\frac{\omega}{c}\right| < |k_x|$. Figure 2(a) shows the absolute value of $\tilde{G}(k_x, y, \omega)$ for $y = 1$ m. The wedge $\left|\frac{\omega}{c}\right| < |k_x|$ containing the traveling wave contributions can be seen clearly. The evanescent contributions are only well visible for the low frequencies due to their rapid decay. Although these contributions decay rapidly, $\tilde{G}(k_x, y, \omega)$ is not strictly bandlimited with respect to the spatial frequency k_x. This holds especially for low frequencies and/or short distances y to the secondary source distribution.

The driving function for the reproduction of a virtual line source is given by (3). For the considered geometry, the driving function is given by two times the partial derivative of (4) with respect to the y-coordinate. Accordingly, its spatial Fourier transform is given by the partial derivative of (7) with respect to y multiplied with $j/2$. This results in

$$\tilde{D}(k_x, \omega) = e^{jk_x x_s} \begin{cases} e^{j\sqrt{(\frac{\omega}{c})^2 - k_x^2}\, y_s} & \text{for } |k_x| < \left|\frac{\omega}{c}\right| , \\ e^{\sqrt{k_x^2 - (\frac{\omega}{c})^2}\, y_s} & \text{for } \left|\frac{\omega}{c}\right| < |k_x| , \end{cases} \tag{9}$$

which is valid for $y_s < 0$. As for the spectrum of the secondary sources (8), the spectrum of the driving function (9) consists of a propagating and an evanescent part. Figure 2(b) shows the absolute value of $\tilde{D}(k_x, \omega)$ for $\mathbf{x}_s = [0 \; -1]$. Note, that the absolute value of $\tilde{D}(k_x, \omega)$ is constant within $|k_x| < \left|\frac{\omega}{c}\right|$. As for the spectrum of the secondary sources, the evanescent contributions for $\left|\frac{\omega}{c}\right| < |k_x|$ decay rapidly. Although these contributions decay rapidly, $\tilde{D}(k_x, \omega)$ is as $\tilde{G}(k_x, y, \omega)$ not bandlimited in the strict sense. This holds especially for low frequencies and/or small distances y_s of the virtual source.

The reproduced wave field for a virtual line source

is given by introducing (8) and (9) into (5)

$$\tilde{P}(k_x, y, \omega) = e^{jk_x x_s} \times$$

$$\times \begin{cases} -\frac{j}{2} \frac{e^{-j\sqrt{(\frac{\omega}{c})^2 - k_x^2}\,(y - y_s)}}{\sqrt{(\frac{\omega}{c})^2 - k_x^2}} & \text{for } |k_x| < \left|\frac{\omega}{c}\right| , \\ \frac{1}{2} \frac{e^{-\sqrt{k_x^2 - (\frac{\omega}{c})^2}\,(y - y_s)}}{\sqrt{k_x^2 - (\frac{\omega}{c})^2}} & \text{for } \left|\frac{\omega}{c}\right| < |k_x| , \end{cases} \tag{10}$$

where the restrictions $y > 0$ and $y_s < 0$ apply. Comparison of (10) with (7) reveals that the field of the desired virtual line source is reproduced perfectly in the listening area ($y > 0$).

Practical implementations of WFS will always be based on spatially discrete secondary sources. Typically, equidistantly spaced loudspeaker arrays are used in WFS. This constitutes a spatial sampling of the continuous secondary source distribution. The consequences of this sampling will be discussed in the remainder of this paper. Here, the introduced spatio-temporal frequency domain representation will play a prominent role.

### 2.3. Spatial Sampling of Secondary Source Distribution

Time-domain sampling is commonly modeled by multiplying a continuous function with a series of Dirac functions [14]. This principle can be applied straightforwardly to sound reproduction. The discretization of the secondary source distribution is modeled by spatial sampling of the driving function. The sampling of the driving function $D(x, \omega)$ is modeled by multiplication with a series of spatial Dirac functions at the positions of the loudspeakers. For an equidistant spacing this reads

$$D_S(x, \omega) = D(x, \omega) \cdot \frac{1}{\Delta x} \sum_{\mu=-\infty}^{\infty} \delta(x - \Delta x \mu) , \tag{11}$$

where $D_S(x, \omega)$ denotes the sampled driving function and Δx the distance (sampling period) between the sampling positions. These positions are indicated in Fig. 1 by the dots $\bullet$. Applying a spatial Fourier transformation to (11) results in

$$\tilde{D}_S(k_x, \omega) = 2\pi \sum_{\eta=-\infty}^{\infty} \tilde{D}\left(k_x - \frac{2\pi}{\Delta x}\eta, \omega\right) . \tag{12}$$

Equation (12) states that the spectrum $\tilde{D}_S(k_x, \omega)$ of the sampled driving function is given as a superposition of the shifted continuous spectrums $\tilde{D}(k_x -$

(a) secondary source spectrum

(b) driving function spectrum
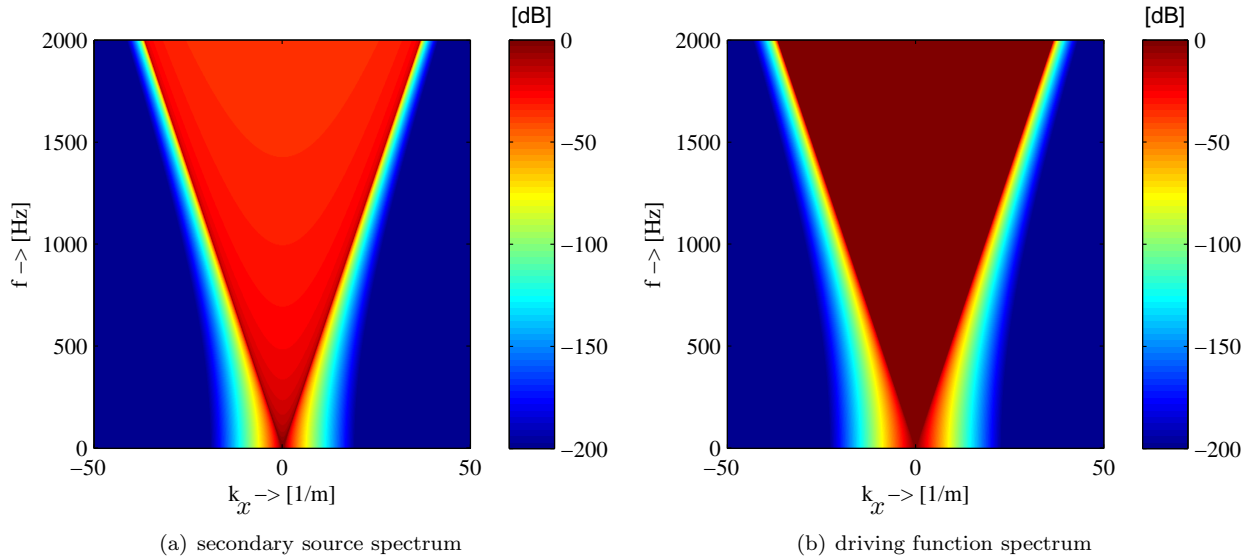
Fig. 2: Spectrum (absolute value) of the secondary sources $\tilde{G}(k_x, y, \omega)$ for $y = 1$ m and driving function $\tilde{D}(k_x, \omega)$ for a virtual source at position $\mathbf{x}_s = [0 \ -1]$ m.

$\frac{2\pi}{\Delta x}\eta, \omega)$ of the driving function. Introducing the spectrum of the sampled driving function into (5) results in the spectrum $\tilde{P}_S(k_x, y, \omega)$ of the wave field reproduced by a spatially discrete secondary source distribution.

In the context of sampling theory, the secondary sources $G(\mathbf{x} - \mathbf{x}_0, \omega)$ can be regarded as an interpolation filter. For time-domain sampling such a filter is typically chosen to provide perfect reconstruction. However for sound reproduction, $G(\mathbf{x} - \mathbf{x}_0, \omega)$ reflects the radiation characteristics and there is only limited freedom for optimization with respect to spatial sampling artifacts.

The theory presented so far assumed a linear secondary source distribution of infinite length along the x-axis. In practice, this distribution will always be of finite length. This truncation has impact on the spatial sampling artifacts of WFS.

3. INFINITE SECONDARY SOURCE DISTRIBUTION

The sampling of a secondary source distribution with infinite length will be discussed first, followed by the specialization to finite length secondary source distributions in the next section.

3.1. General Considerations

The reproduced wave field $\tilde{P}_S(k_x, y, \omega)$ for an infinitely long secondary source distribution is given by weighting the spectrum of the sampled driving function $\tilde{D}_S(k_x, \omega)$ with the spectrum of the secondary sources $\tilde{G}(k_x, y, \omega)$. The spectrum of the sampled driving function is given by a superposition of the shifted spectra of the continuous driving function. Qualitatively, artifacts due to the secondary source sampling can only be avoided when

1. the spectrum of the driving function is bandlimited, and

2. the spectrum of the secondary sources is bandlimited.

Due to sampling, the spectrum of the continuous driving function is repeated with an interval of $2\pi/\Delta x$ on the k_x-axis. The first condition ensures that there exists a sampling interval Δx (loudspeaker distance) where no spectral overlaps occur in the sampled driving function, the second condition ensures that the spectral repetitions in the sampled driving function will be filtered out by the characteristics of the secondary sources.

The first type of artifacts is known as *spatial aliasing*, while the second type of artifacts can be interpreted as reconstruction errors. We will threat both as spatial sampling artifacts in the remainder.

3.2. Qualitative Analysis

The driving function for the reproduction of a virtual line source is given by (9) and illustrated in Fig. 2(b). It was already concluded in Section 2.2 that $\tilde{D}(k_x, \omega)$ is not bandlimited in the strict sense. However, for a fixed frequency ω, the propagating part is bandlimited with respect to k_x. The evanescent part is not bandlimited but rapidly decaying with increasing distance y_s of the virtual source to the secondary source contour. Hence, the first condition given above is not strictly fulfilled for the evanescent contributions in $\tilde{D}(k_x, \omega)$.

The spectrum of the secondary line sources is given by (8) and illustrated in Fig. 2(a). As for the driving function, $\tilde{G}(k_x, y, \omega)$ is also not strictly bandlimited. However, the propagating part is bandlimited and the evanescent part is rapidly decaying over distance y to the secondary sources. Hence, the second condition given above is not strictly fulfilled for the evanescent contributions.

Summarizing, neither the spectrum of the driving function for a virtual line source nor the spectrum of the secondary source are strictly bandlimited. In order to understand the influence of the non-bandlimited contributions a detailed analysis will be performed in the following.

Figure 3 illustrates, on a qualitative level, the computation of the spectrum of the reproduced wave field $\tilde{P}_S(k_x, y, \omega)$ for a sampled secondary source distribution. The dark gray areas denote the propagating parts of the driving function $\tilde{D}_S(k_x, \omega)$ and the secondary sources $\tilde{G}(k_x, y, \omega)$, respectively, the light gray areas the evanescent contributions. Four different types of overlaps between the spectrum of the sampled driving function and the secondary source can be identified. These are discussed in the following.

3.3. Propagating Contributions

The propagating contributions of the reproduced wave field are given by the propagating contribution of the secondary sources $\tilde{G}(k_x, y, \omega)$ in conjunction with the propagating and evanescent contributions of the driving function $\tilde{D}_S(k_x, \omega)$. Hence, two propagating contributions are present.

The first propagating contribution is given by the overlaps between the propagating contributions of both $\tilde{D}_S(k_x, \omega)$ and $\tilde{G}(k_x, y, \omega)$. Both are bandlimited for a given frequency ω of the virtual line source. However, if the sampling interval Δx of the secondary sources gets too small the propagating parts will overlap in the sampled driving function. For this situation an anti-aliasing condition can be derived easily from Fig. 3. It is given as

$$f_{\mathrm{al}} \leq \frac{c}{2\Delta x} \ , \qquad (13)$$

where f_{al} denotes the (maximum) frequency of the virtual source where no spatial aliasing is present. Hence, for this propagating contribution aliasing can be avoided by limiting either the temporal bandwidth of the virtual source or decreasing the sampling interval between the secondary sources (loudspeakers). The reproduced wave field for the first propagating part is given as

$$\tilde{P}_{S,\mathrm{pr1}}(k_x, y, \omega) = j\pi \, \frac{e^{-j\sqrt{(\frac{\omega}{c})^2 - k_x^2}\, y}}{\sqrt{(\frac{\omega}{c})^2 - k_x^2}} \times$$
$$\times \sum_{\eta'} e^{j(k_x - \eta\frac{2\pi}{\Delta x})x_s} e^{j\sqrt{(\frac{\omega}{c})^2 - (k_x - \eta\frac{2\pi}{\Delta x})^2}\, y_s} \ , \quad (14)$$

for $|k_x| < \left|\frac{\omega}{c}\right|$ and for those η' where $\left|k_x - \eta'\frac{2\pi}{\Delta x}\right| < \left|\frac{\omega}{c}\right|$ is fulfilled for a given frequency ω.

A second propagating contribution emerges when the evanescent contributions of the driving function $\tilde{D}_S(k_x, \omega)$ overlap with the propagating contributions of the secondary sources. It is given as

$$\tilde{P}_{S,\mathrm{pr2}}(k_x, y, \omega) = j\pi \, \frac{e^{-j\sqrt{(\frac{\omega}{c})^2 - k_x^2}\, y}}{\sqrt{(\frac{\omega}{c})^2 - k_x^2}} \times$$
$$\times \sum_{\eta'} e^{j(k_x - \eta\frac{2\pi}{\Delta x})x_s} e^{\sqrt{(k_x - \eta\frac{2\pi}{\Delta x})^2 - (\frac{\omega}{c})^2}\, y_s} \ , \quad (15)$$

for $|k_x| < \left|\frac{\omega}{c}\right|$ and for those η' where $\left|k_x - \eta\frac{2\pi}{\Delta x}\right| > \left|\frac{\omega}{c}\right|$ is fulfilled for a given frequency ω. No strict anti-aliasing contribution can be given for $\tilde{P}_{S,\mathrm{pr2}}(k_x, y, \omega)$, since the evanescent part of the driving function $\tilde{D}_S(k_x, \omega)$ is not bandlimited. This contribution can be interpreted as side effect of spatial sampling. However, its energy will be quite low in typical situations due to the rapid decay of the evanescent contributions.
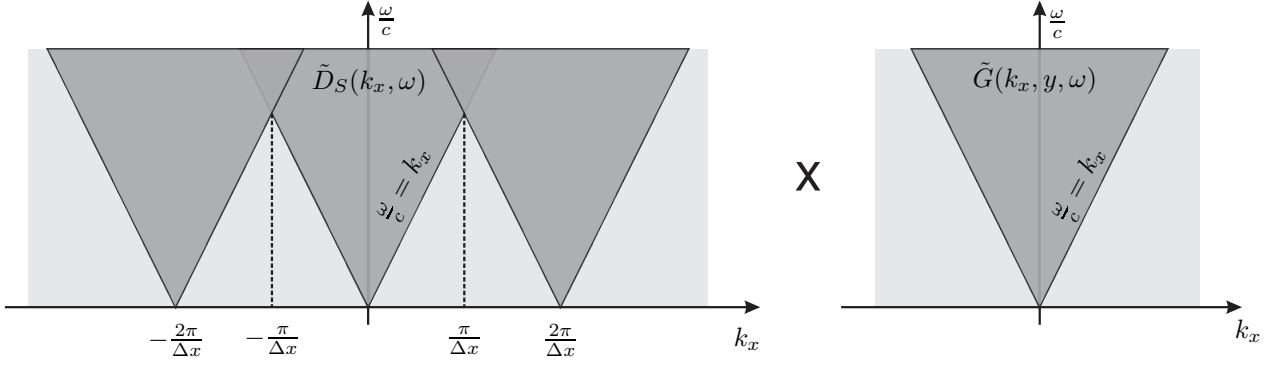
Fig. 3: Qualitative illustration of the computation of the spectrum of the reproduced wave field $\tilde{P}_S(k_x, y, \omega)$ for a sampled secondary source distribution. The dark gray areas denote the propagating parts, the light gray areas the evanescent.

3.4. Evanescent Contributions

As for the propagating parts, two evanescent contributions can be identified in the reproduced wave field. The first one is given by the overlaps of the propagating parts of the driving function with the evanescent parts of the secondary sources. It is given as

$$\tilde{P}_{S,\mathrm{ev1}}(k_x, y, \omega) = -\pi \frac{e^{-\sqrt{k_x^2 - (\frac{\omega}{c})^2}\, y}}{\sqrt{k_x^2 - (\frac{\omega}{c})^2}} \times$$
$$\times \sum_{\eta'} e^{j(k_x - \eta \frac{2\pi}{\Delta x}) x_s} e^{j\sqrt{(\frac{\omega}{c})^2 - (k_x - \eta \frac{2\pi}{\Delta x})^2}\, y_s} \;, \quad (16)$$

for $|k_x| < \left|\frac{\omega}{c}\right|$ and for those η' where $\left|k_x - \eta' \frac{2\pi}{\Delta x}\right| < \left|\frac{\omega}{c}\right|$ is fulfilled for a given frequency ω. Equation (16) describes a traveling wave in x-direction and an evanescent wave in y-direction.

The second evanescent contribution is given by the overlaps of the evanescent parts of the driving function and the secondary sources. It is given as

$$\tilde{P}_{S,\mathrm{ev2}}(k_x, y, \omega) = -\pi \frac{e^{-\sqrt{k_x^2 - (\frac{\omega}{c})^2}\, y}}{\sqrt{k_x^2 - (\frac{\omega}{c})^2}} \times$$
$$\times \sum_{\eta'} e^{j(k_x - \eta \frac{2\pi}{\Delta x}) x_s} e^{\sqrt{(k_x - \eta \frac{2\pi}{\Delta x})^2 - (\frac{\omega}{c})^2}\, y_s} \;, \quad (17)$$

for $|k_x| > \left|\frac{\omega}{c}\right|$ and for those η' where $\left|k_x - \eta \frac{2\pi}{\Delta x}\right| > \left|\frac{\omega}{c}\right|$ is fulfilled for a given frequency ω.
No strict anti-aliasing contribution can be derived for both evanescent contributions $\tilde{P}_{S,\mathrm{ev1}}(k_x, y, \omega)$ and $\tilde{P}_{S,\mathrm{ev2}}(k_x, y, \omega)$ since the evanescent part of the
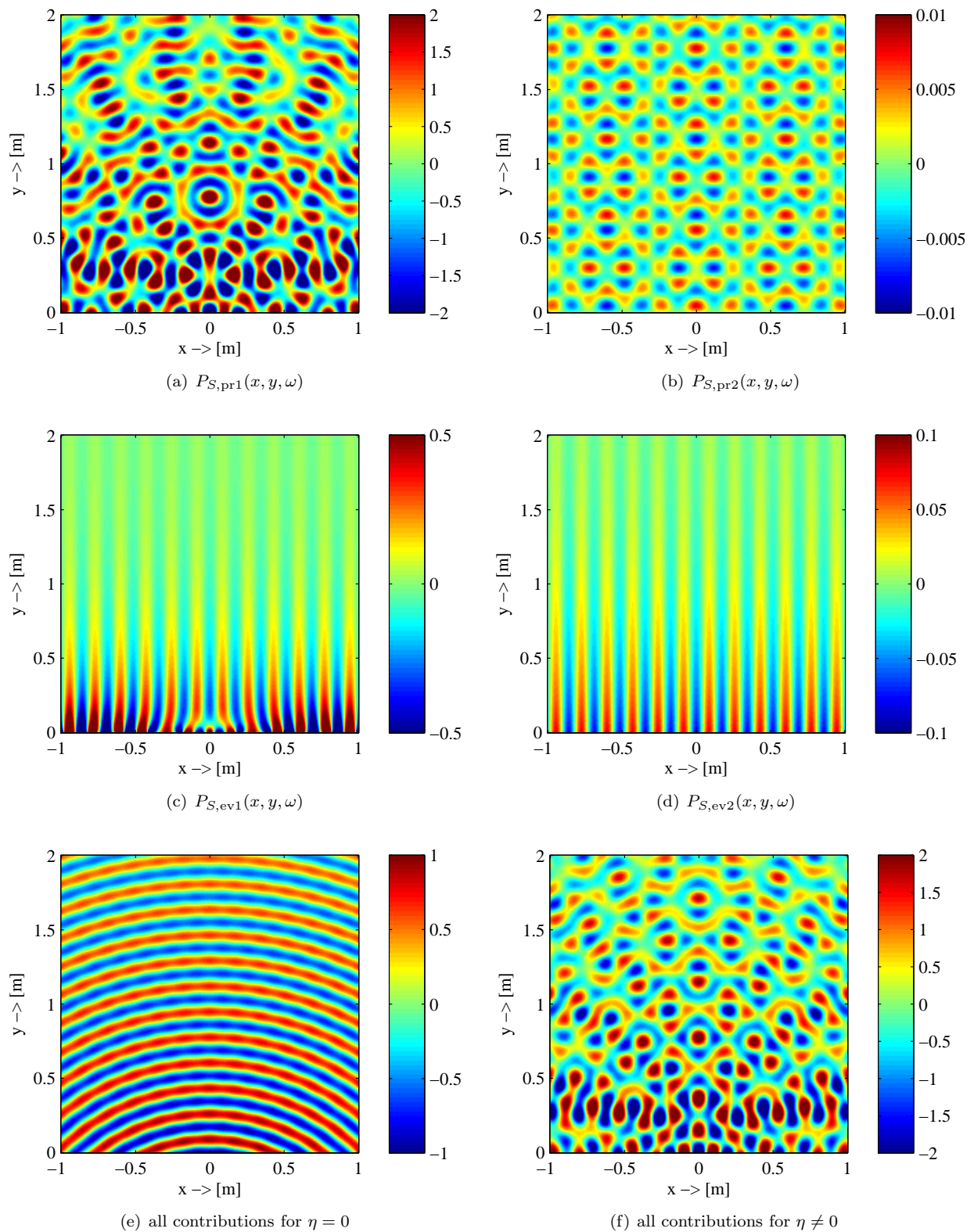
secondary sources $\tilde{G}(k_x, y, \omega)$ is not strictly bandlimited. As for the propagating part $\tilde{P}_{S,\mathrm{pr2}}(k_x, y, \omega)$, these contributions can be interpreted as a side effect of spatial sampling.

A simulated example is discussed in the next subsection in order to illustrate the different contributions to the reproduced wave field derived in this and the previous subsection.

3.5. Example

The reproduction of a monochromatic virtual line source with a frequency of $f_s = 2000$ Hz placed at the position $\mathbf{x}_s = [0 \, {-}1]^T$ m is considered. The sampling interval of the secondary sources is chosen to $\Delta x = 0.20$ m, a value that is typical for WFS setups. Equations (14), (15), (16) and (17) have been evaluated numerically in MATLAB. The resulting spectra have then been transformed back into the spatial domain by applying an inverse Fourier transform. Figure 4 shows the results (real part of the wave fields). Note the different color scales used to highlight the structure of the wave fields.

Figures 4(a) to 4(d) illustrate the two propagating and the two evanescent contributions. Figure 4(a) shows the propagating part $P_{S,\mathrm{pr1}}(x, y, \omega)$ as given by Eq. (14). The aliasing artifacts, due to the overlap of the propagating parts in the driving function, are clearly visible. The aliasing frequency for the simulated scenario is $f_{\mathrm{al}} \approx 850$ Hz. Figure 4(b) illustrates the second propagating contribution $P_{S,\mathrm{pr2}}(x, y, \omega)$, as given by Eq. (15). Note the different color scale used. This part has a relatively low level compared to $P_{S,\mathrm{pr1}}(x, y, \omega)$. This is

(a) $P_{S,\mathrm{pr1}}(x,y,\omega)$

(b) $P_{S,\mathrm{pr2}}(x,y,\omega)$

(c) $P_{S,\mathrm{ev1}}(x,y,\omega)$

(d) $P_{S,\mathrm{ev2}}(x,y,\omega)$

(e) all contributions for $\eta = 0$

(f) all contributions for $\eta \neq 0$

Fig. 4: Numerical simulation of the four contributions for the reproduction of a virtual line source ($\mathbf{x}_s = [0 \; -1]^T$ m, $f_s = 2000$ Hz, $\Delta x = 0.20$ m) and superposition of all contributions for $\eta = 0$ and $\eta \neq 0$.

due to the rapid decay of the evanescent contribution in Eq. (15). However, the level of $P_{S,\mathrm{pr2}}(x,y,\omega)$ will increase for virtual source positions close to the secondary source distribution.

Figures 4(c) and 4(d) show the two evanescent contributions $P_{S,\mathrm{ev1}}(x,y,\omega)$ and $P_{S,\mathrm{ev2}}(x,y,\omega)$ as given by (16) and (17). Their exponential decay with distance to the secondary source distribution can be seen clearly. Note the different color scales used. The reproduced wave field $P_S(x,y,\omega)$ for the simulated scenario is a superposition of the wave fields shown in Fig. 4(a) to 4(d).

Alternatively to the decomposition into the four contributions discussed above, it is also possible to split the reproduced wave field into two parts. One that considers only the terms for $\eta = 0$, and one that considers only the spectral repetitions by evaluating and summing up all terms for $\eta \neq 0$. The first part can be interpreted as the desired wave field, while the second one holds the spatial sampling artifacts. Figure 4(e) shows the reproduced wave field for $\eta = 0$. The wave field matches the desired field of the virtual line source at the chosen position. Figure 4(f) shows the aliasing contributions by evaluating only the terms for $\eta \neq 0$. Severe aliasing contributions can be seen here. The reproduced wave field is again given by superimposing the wave fields in Fig. 4(e) and 4(f).

3.6. Summary

The detailed analysis of the wave field reproduced by a sampled secondary source distribution for the reproduction of a virtual line source revealed a number of interesting insights. The reproduced wave field can be decomposed into four contributions, from which two are evanescent waves. A strict anti-aliasing condition can only be derived for the first propagating part $\tilde{P}_{\mathrm{pr1}}(k_x,y,\omega)$. The condition (13) states that the temporal bandwidth of the virtual source has to be limited accordingly to the sampling interval of the secondary sources. No strict anti-aliasing condition can be derived for the other three contributions. Interestingly, these contributions are a side effect of spatial sampling of the secondary source distribution. They are not present for a continuous secondary source distribution.

The loudspeaker distances Δx chosen in practical implementations results in anti-aliasing frequencies that are very low (some few kHz) compared to the

typical bandwidth of 20 kHz used in high-quality audio reproduction. It has been shown, that the resulting spatial aliasing has less impact on the perceptual quality of WFS as one could assume when performing a detailed analysis of the reproduced wave field [4]. However, spatial aliasing may result in perceivable coloration of the virtual source. The presented results could help to understand the influence of spatial aliasing better.

4. TRUNCATED SECONDARY SOURCE DISTRIBUTION

Up to now, the linear secondary source distribution was assumed to be of infinite length in the x-direction. However, practical implementations of linear loudspeaker arrays will always be of finite length. The impact of this truncation on the spatial sampling artifacts is derived in the following subsections.

4.1. Truncated Driving Function

Truncation can be modeled by multiplying the secondary source driving function $D(x_0,\omega)$ with a suitable window function $w(x_0)$ [7]. Incorporating $w(x_0)$ into Eq. (1) yields the wave field $P_{\mathrm{tr}}(\mathbf{x},\omega)$ reproduced by a truncated linear array as

$$P_{\mathrm{tr}}(\mathbf{x},\omega) = \\ -\int_{-\infty}^{\infty} w(x_0)D(\mathbf{x}_0,\omega)\, G(\mathbf{x}-\mathbf{x}_0,\omega)\ dx_0 \ . \quad (18)$$

Spatial Fourier transformation of $P_{\mathrm{tr}}(\mathbf{x},\omega)$ yields the spectrum of the reproduced wave field as

$$\tilde{P}_{\mathrm{tr}}(k_x,y,\omega) = \\ -\frac{1}{2\pi}\underbrace{\left(\tilde{w}(k_x) *_{k_x} \tilde{D}(k_x,\omega)\right)}_{\tilde{D}_{\mathrm{tr}}(k_x,\omega)} \tilde{G}(k_x,y,\omega)\ , \quad (19)$$

where $*_{k_x}$ denotes convolution with respect to the spatial frequency k_x and $\tilde{w}(k_x)$ the spatial Fourier transform of $w(x)$. A secondary source distribution with finite length L can be modeled by a rectangular window function. In this case, the window function $w(x)$ is given by the rect-function [14]

$$w(x) = \mathrm{rect}\left(\frac{x}{L}\right) = \begin{cases} 1 & \text{, if } |x| \leq \frac{L}{2}\ , \\ 0 & \text{, otherwise }\ , \end{cases} \quad (20)$$

for $L > 0$. The spatial Fourier transformation of $w(x)$ with respect to the x-variable is given as

$$\tilde{w}(k_x) = L \, \frac{\sin(\frac{k_x}{2}L)}{\frac{k_x}{2}L} = L \, \text{sinc}(\frac{k_x}{2}L) \, . \qquad (21)$$

The driving function for a truncated secondary source distribution is given by convolving $\tilde{w}(k_x)$ with the driving function $\tilde{D}(k_x, \omega)$. The driving function for a virtual line source is given by (9). Although this driving function does not involve very complex mathematical expressions, the analytical evaluation of the convolution integral is quite complex and will not be performed here.

Figure 5 shows the result of numerical evaluation of the convolution for two exemplary virtual source positions. Comparison with Fig. 2(b) reveals that the energy of the truncated driving function $\tilde{D}_{\text{tr}}(k_x, \omega)$ is concentrated in a smaller region than for the infinite length secondary source distribution. This holds especially for the second position $\mathbf{x}_{s2}$ shown in Fig. 5(b). Besides these differences on a more coarse level, also differences in the fine structure can be observed in Fig. 5 (e.g. ripples). Other window functions can be applied to limit these effects [7].

The concentration of energy, that can be exhibited for the truncated driving function $\tilde{D}_{\text{tr}}(k_x, \omega)$, has influence on the occurrence of spatial sampling artifacts. This is evident when comparing the finite and infinite length case as, illustrated in Fig. 5 and 3. In order to derive the effects of spatial sampling and approximate anti-aliasing conditions for truncated secondary source distributions, a geometric approximation will be applied in conjunction with an decomposition of the driving function into plane waves. It was derived in Section 3.3, that an anti-aliasing condition can only be given for the propagating part $\tilde{P}_{\text{pr1}}(k_x, y, \omega)$ of the reproduced wave field. Hence, we will only consider this part for the derivation of the anti-aliasing conditions.

4.2. Geometric Approximation

The truncation of the secondary source distribution leads to a limited listening area [7, 5]. The resulting listening area, for a given position of the virtual source, can be approximated quite well by simple geometric means. This approximation states that a virtual line source will be reproduced almost correctly in a wedge in front of the array. The boundary of this wedge shaped area is given by connecting the
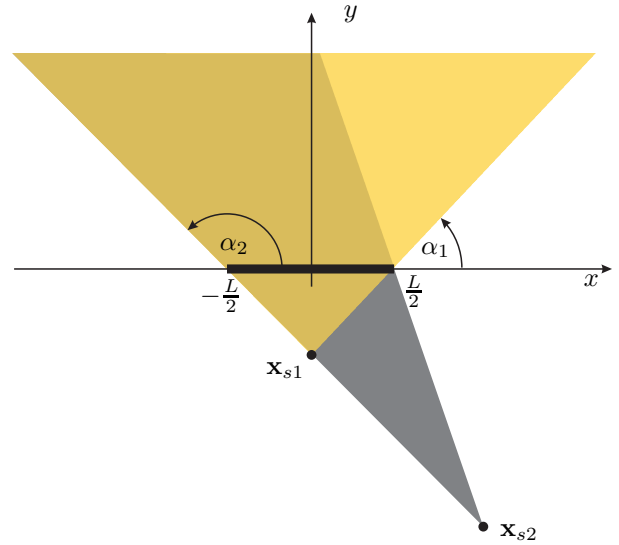
Fig. 6: Approximation of listening area (shown by yellow and gray wedge) for reproduction of a virtual line source with a truncated linear array.

position of the virtual line source with the endings of the truncated secondary source distribution. This is illustrated in Fig. 6 for the same virtual source positions as used in Fig. 5. Outside of this area the energy of the reproduced wave field will be quite low. Inside of this area the reproduced wave field will approximately match the virtual source wave field when neglecting sampling. The angles α_1 and α_2 of the sides of the wedge (see Fig. 6) are given as

$$\tan \alpha_1 = \frac{-y_s}{\frac{L}{2} - x_s} \, , \qquad (22a)$$

$$\tan(\alpha_2 - \frac{\pi}{2}) = \frac{\frac{L}{2} + x_s}{-y_s} \, , \qquad (22b)$$

where $0 \le \alpha_1, \alpha_2 < \pi$ and $\alpha_1 \le \alpha_2$. The geometric approximation of the listening area is now brought into conjunction with the effect of truncation on the driving function.

Arbitrary acoustic wave fields can be represented as a superposition of plane waves [8]. This technique is also known as *plane wave decomposition* [15, 16]. The plane wave contributions of the driving function $\tilde{D}_{\text{tr}}(k_x, \omega)$ can be derived by substituting k_x with [17, 16]

$$k_x = \frac{\omega}{c} \cos \alpha \, , \qquad (23)$$

(a) $\mathbf{x}_{s1} = [0 \; -1]^T$ m   (b) $\mathbf{x}_{s2} = [2 \; -3]^T$ m
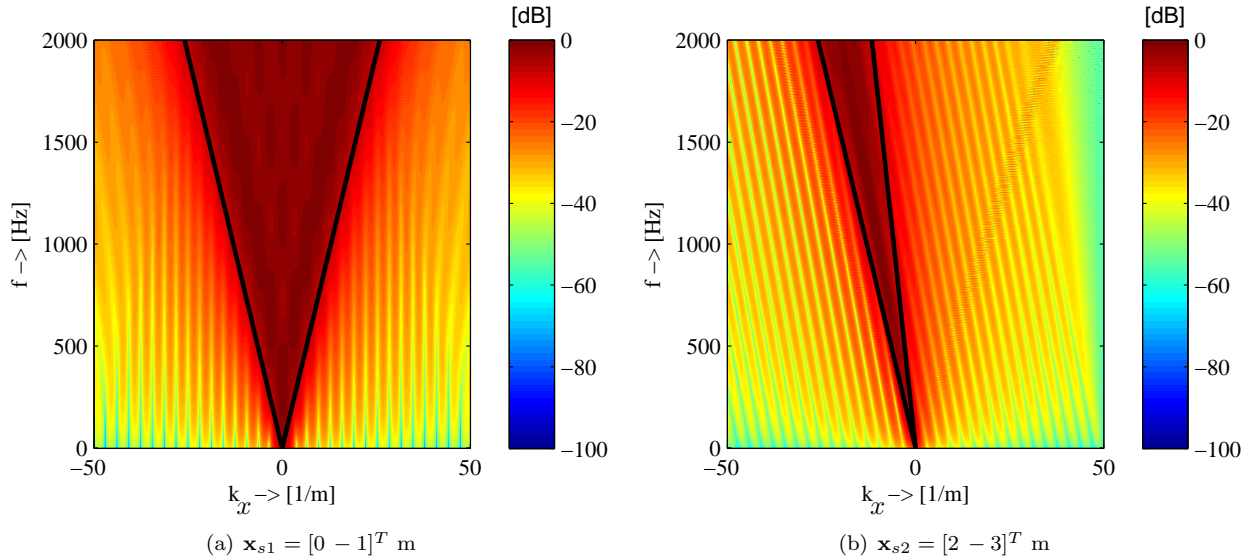
Fig. 5: Spectrum (absolute value) of truncated driving function $\tilde{D}_{\mathrm{tr}}(k_x, \omega)$ and geometric approximation of its main contributions for a length of the secondary source distribution of $L = 2$ m.

where α denotes the incidence angle of the plane wave. Hence, the spectrum of a plane wave with given incidence angle α is given by the spectral components collected along a tilted line in the k_x-ω spectrum. Applying this interpretation to Fig. 2(b), showing the driving function $\tilde{D}(k_x, \omega)$ without truncation, discloses that all plane wave contributions for $0 < \alpha < \pi$ are present with equal level.

The geometric approximation of the listening area, for a truncated secondary source distribution, states that the major plane wave contributions of the driving function $\tilde{D}_{\mathrm{tr}}(k_x, \omega)$ will be limited within the angles α_1 and α_2. These limits are shown, for the two exemplary source positions, in Fig. 5 by the black lines. It can be seen clearly that the main energy in the driving function is within these angles. Hence, the geometric approximation provides a reasonable approximation of the effects imposed by the truncation to the driving function.

4.3. Anti-Aliasing Conditions
The truncated and sampled driving function $\tilde{D}_{\mathrm{tr},S}(k_x, \omega)$ is given by introducing the truncated driving function $\tilde{D}_{\mathrm{tr}}(k_x, \omega)$ into (12). Hence, spectral repetitions will result due to the sampling. The reproduced wave field is given by multiplying the truncated and sampled driving function $\tilde{D}_{\mathrm{tr},S}(k_x, \omega)$

with the secondary source spectrum $\tilde{G}(k_x, y, \omega)$. Figure 7 illustrates the calculation of the reproduced wave field for two different spatial sampling intervals Δx. The dark gray wedges illustrate the truncated and sampled driving function $\tilde{D}_{S,\mathrm{tr}}(k_x, \omega)$, the light gray wedges the secondary source spectrum $\tilde{G}(k_x, y, \omega)$. The geometric approximation of the propagating part of the driving function, as discussed in the previous subsection, has been applied. It can be concluded from Fig. 7 that two different types of overlaps between the spectra of the driving function and the secondary sources can be identified. These are

1. the spectral repetitions of the driving function overlap with the secondary source spectrum, and

2. the repetitions of the driving function overlap.

Both types of sampling artifacts will result in additional contributions beside the desired virtual source. The first type of artifacts will result in plane wave contributions with different incidence angles than the virtual source, the second type in plane wave contributions that interfere with the plane wave contributions of the virtual source. Hence,

(a) no overlap of spectral repetitions of driving function

(b) overlap of spectral repetitions of driving function
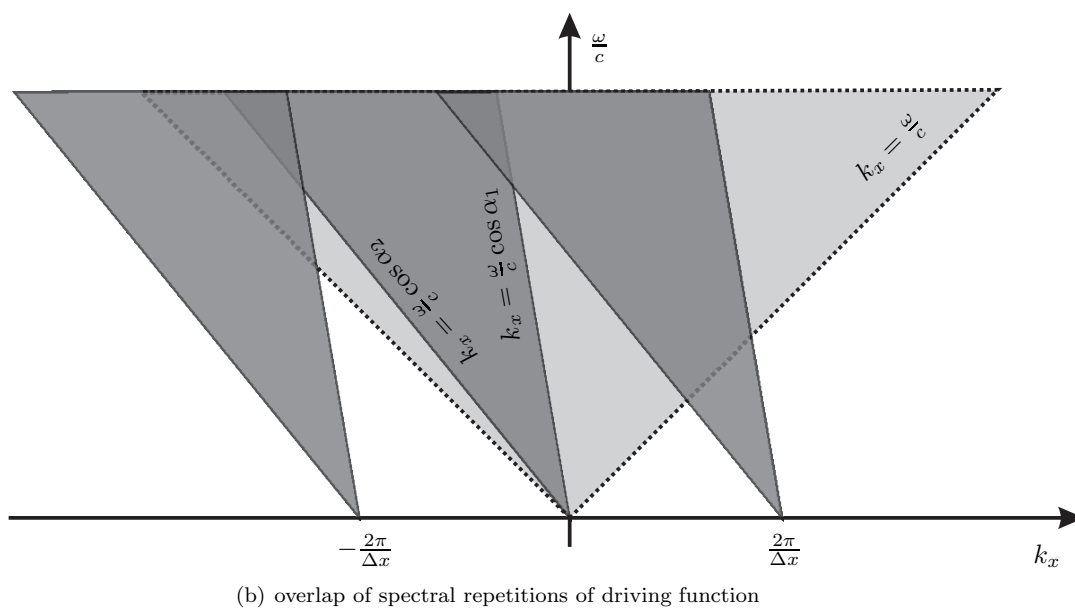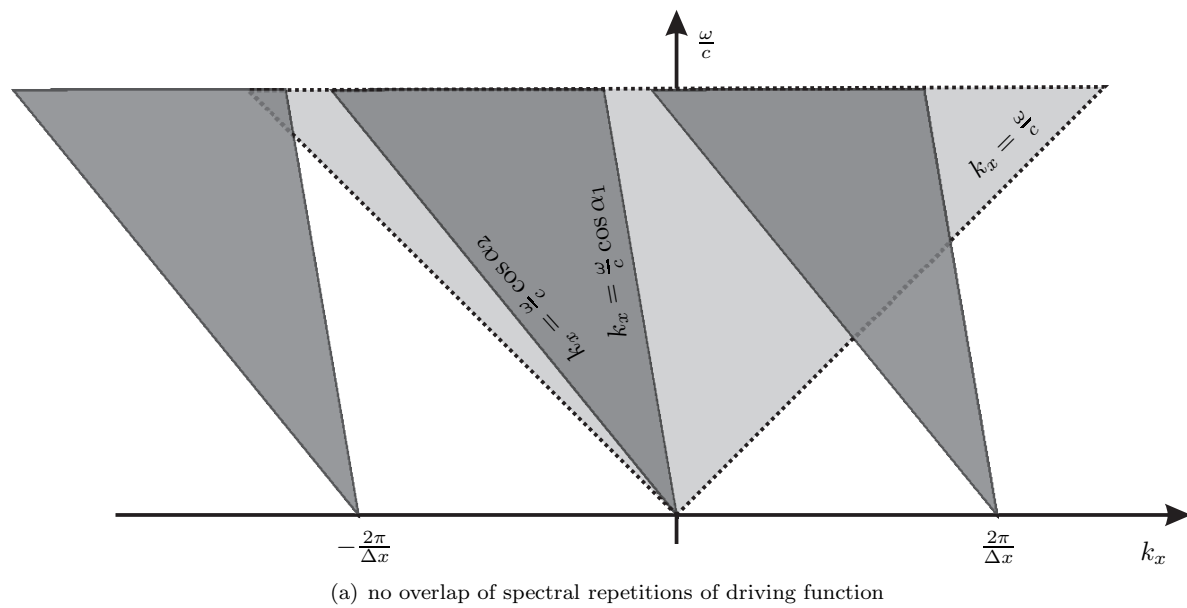
Fig. 7: Qualitative illustration of the computation of the spectrum of the reproduced wave field for a sampled and truncated secondary source distribution. The light gray areas illustrate the secondary source spectrum $\tilde{G}(k_x, y, \omega)$, while the dark gray areas illustrate the spectrum $\tilde{D}_{S,\mathrm{tr}}(k_x, \omega)$ of the driving function.

when considering the limited listening area for a truncated secondary source distribution, the first type of sampling artifacts will not be present within the listening area for listener positions far away from the secondary source distribution. Consequently, the occurrence of the first type of sampling artifacts will depend on the listener position.

The spectral repetitions of the driving function $\tilde{D}_{\text{tr},S}(k_x, \omega)$ will overlap with the secondary source spectrum $\tilde{G}(k_x, y, \omega)$ when one of the following two conditions is satisfied

$$f_1 \leq \frac{c}{\Delta x(1 - \cos \alpha_2)} \; , \qquad (24\text{a})$$

$$f_2 \leq \frac{c}{\Delta x(1 + \cos \alpha_1)} \; . \qquad (24\text{b})$$

The spatial aliasing frequency $f_{\text{tr,al1}}$ for the reproduction of a virtual line source by a finite length secondary source distribution is given by the smaller value of f_1 and f_2.

A higher aliasing frequency can be derived for listener positions within the listening area of the virtual source which are far away from the secondary source positions. By analyzing the geometry in Fig. 7(b) this frequency can be derived as

$$f_{\text{tr,al2}} \leq \frac{c}{\Delta x(\cos \alpha_1 - \cos \alpha_2)} \; , \qquad (25)$$

for $\alpha_1 \neq \alpha_2$. The spatial aliasing frequency for arbitrary listener positions within the listening area will lie between the two limits $f_{\text{tr,al1}}$ and $f_{\text{tr,al2}}$ depending on the actual position. It can be concluded furthermore that $f_{\text{al}} \leq f_{\text{tr,al1}} \leq f_{\text{tr,al2}}$.

The spatial aliasing frequency will be infinite, according to (25), for virtual source and listener positions far away from the secondary source distribution ($y_s \to -\infty$, $y \to \infty$). This is equivalent to the reproduction of a plane wave with a truncated secondary source distribution, as discussed in [3].

For a secondary source distribution with infinite length, both conditions (24) and (25) become equal to (13).

4.4. Example
An example for the application of the anti-aliasing conditions for a truncated and sampled secondary source contour is given in the following. The reproduction of a monochromatic line source placed at $\mathbf{x}_s = [0 \; -1]^T$ m on a loudspeaker array with a spacing of $\Delta x = 0.20$ m consisting of 16 line sources is
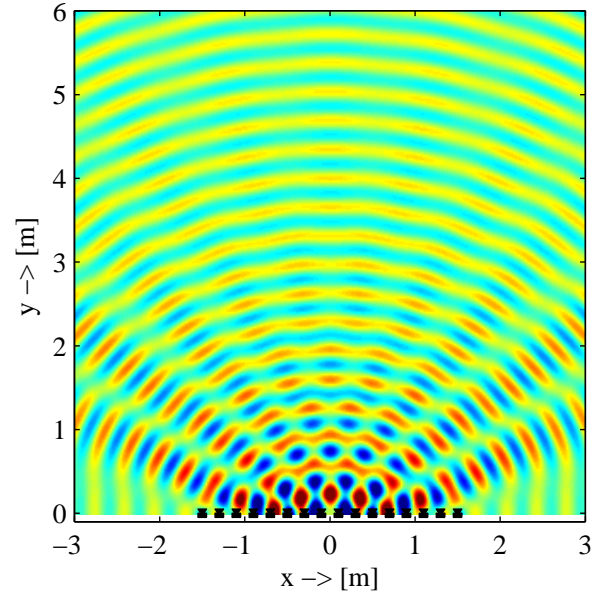
Fig. 8: Wave field reproduced for a virtual point source ($\mathbf{x}_s = [0 \; -1]^T$ m, $f_s = 1000$ Hz by a loudspeaker array ($\Delta x = 0.20$ m) with 16 loudspeakers.

considered. The total length is $L = 3$ m. The angles limiting the reproduction area can be derived from (22) as $\alpha_1 \approx 33.7°$ and $\alpha_2 \approx 146.3°$. The anti-aliasing limits are $f_1 = f_2 = f_{\text{tr,al1}} \approx 936.1$ Hz and $f_{\text{tr,al2}} \approx 1030.6$ Hz. In order to show the position dependency of the aliasing contributions a frequency in between the two anti-aliasing conditions of $f_s = 1000$ Hz has been chosen for the virtual line source. Figure 8 shows the reproduced wave field for the considered scenario. It can be seen clearly, besides the truncation artifacts [7], that the aliasing artifacts are quite dominant for positions close to the loudspeakers. For listener positions with some distance to the loudspeakers these artifacts are not present.

5. CONCLUSION
This paper presents a detailed analysis of the spatial sampling artifacts of two-dimensional WFS for the reproduction of virtual line sources. The rigid formulation of the sampling process revealed a number of interesting insights. One of these is, that spatial sampling results in evanescent contributions that are not present without spatial sampling. The authors

are not aware of work considering the perception of evanescent waves by humans. Hence, the perceptual relevance of these contributions is not clear to the authors at the current stage.

Anti-aliasing conditions have been derived for infinitely long and truncated secondary source distributions. These state that the temporal bandwidth of the virtual source has to be limited in order to avoid sampling artifacts. It was further shown, that for secondary source distributions with finite length, the spatial sampling artifacts depend on the listener position. Note, that the transition between no spatial aliasing and spatial aliasing will not be hard with increasing frequency of the virtual source due to the evanescent contributions and truncation artifacts.

The derived anti-aliasing conditions will also hold for the more practical case of 2.5D reproduction using secondary point sources. However, the exact formulation of the different contributions to the reproduced wave field might be different. A detailed analysis will be performed in the future.

The results derived in this paper may help to understand the perception of spatial aliasing artifacts and near-field effects. Subjective experiments are planned in the future. The analytic expressions derived for the anti-aliasing conditions are also useful in designing improved pre-equalization filters [7, 6] for WFS. The energy added to the high-frequency regions by the spatial overlaps has to be considered in the filter design.

6. REFERENCES

[1] D. Leckschat and M. Baumgartner. Wellenfeldsynthese: Untersuchungen zu Alias-Artefakten im Ortsfrequenzbereich und Realisierung eines praxistauglichen WFS-Systems. In *31. Deutsche Jahrestagung für Akustik*, Munic, Germany, 2005.

[2] S. Spors. Spatial aliasing artifacts produced by linear loudspeaker arrays used for wave field synthesis. In *Second IEEE-EURASIP International Symposium on Control, Communications, and Signal Processing*, Marrakech, Morocco, March 2006.

[3] S. Spors and R. Rabenstein. Spatial aliasing artifacts produced by linear and circular loudspeaker arrays used for wave field synthesis. In *120th AES Convention*, Paris, France, May 2006. Audio Engineering Society (AES).

[4] H. Wittek. *Perceptual differences between wavefield synthesis and stereophony*. PhD thesis, University of Surrey, 2007.

[5] A.J. Berkhout, D. de Vries, and P. Vogel. Acoustic control by wave field synthesis. *Journal of the Acoustic Society of America*, 93(5):2764–2778, May 1993.

[6] S. Spors, R. Rabenstein, and J. Ahrens. The theory of wave field synthesis revisited. In *124th AES Convention*, Amsterdam, The Netherlands, May 2008. Audio Engineering Society (AES).

[7] E.W. Start. *Direct Sound Enhancement by Wave Field Synthesis*. PhD thesis, Delft University of Technology, 1997.

[8] E.G. Williams. *Fourier Acoustics: Sound Radiation and Nearfield Acoustical Holography*. Academic Press, 1999.

[9] M. Abramowitz and I.A. Stegun. *Handbook of Mathematical Functions*. Dover Publications, 1972.

[10] S. Spors, M. Renk, and R. Rabenstein. Limiting effects of active room compensation using wave field synthesis. In *118th AES Convention*, Barcelona, Spain, May 2005. Audio Engineering Society (AES).

[11] J. Ahrens and S. Spors. Sound field reproduction using planar and linear arrays of loudspeakers. *IEEE Transactions on Audio, Speech and Signal Processing*, 2009. Submitted.

[12] J. Ahrens and S. Spors. Reproduction of a plane-wave sound field using planar and linear arrays of loudspeakers. In *Third IEEE-EURASIP International Symposium on Control, Communications, and Signal Processing*, March 2008.

[13] I.S. Gradshteyn and I.M. Ryzhik. *Tables of Integrals, Series, and Products*. Academic Press, 2000.

[14] B. Girod, R. Rabenstein, and A. Stenger. *Signals and Systems*. J.Wiley & Sons, 2001.

[15] E. Hulsebos, D. de Vries, and E. Bourdillat. Improved microphone array configurations for auralization of sound fields by Wave Field Synthesis. In *110th AES Convention*, Amsterdam, Netherlands, May 2001. Audio Engineering Society (AES).

[16] S. Spors. *Active Listening Room Compensation for Spatial Sound Reproduction Systems*. PhD thesis, University of Erlangen-Nuremberg, 2006.

[17] R. Rabenstein, P. Steffen, and S. Spors. A tutorial on the representation of two-dimensional wave fields by multidimensional signals. In *4th International Workshop on (ND) Multidimensional Systems*, Wuppertal, Germany, July 2005.